CSIRO PUBLISHING

Australian Journal of Physics

Volume 52, 1999

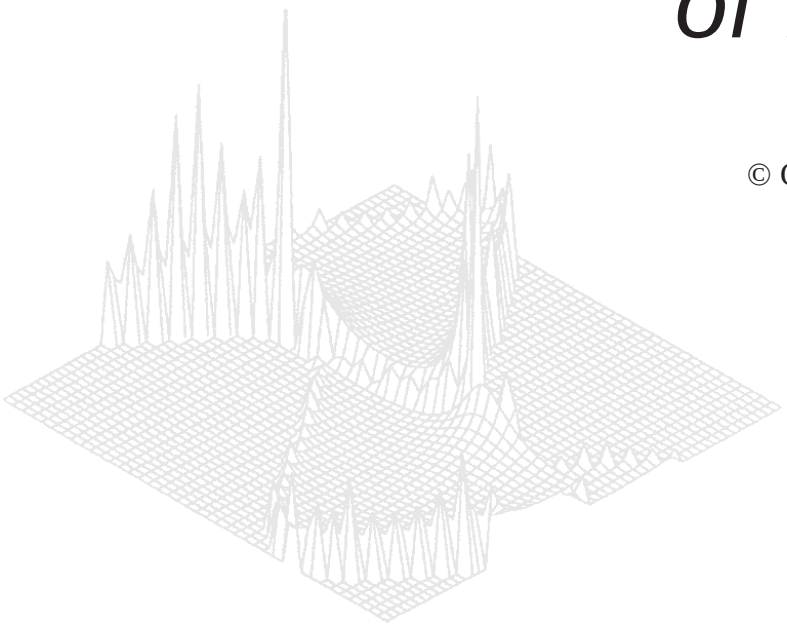

A journal for the publication of
original research in all branches of physics

www.publish.csiro.au/journals/ajp

All enquiries and manuscripts should be directed to
Australian Journal of Physics
CSIRO PUBLISHING
PO Box 1139 (150 Oxford St)
Collingwood Telephone: 61 3 9662 7626
Vic. 3066 Facsimile: 61 3 9662 7611
Australia Email: peter.robertson@publish.csiro.au

Published by **CSIRO** PUBLISHING
for CSIRO Australia and
the Australian Academy of Science

Aust. J. Phys., 1999, **52**, 1–26

Twinkle, Twinkle Little Pulsar/Quasar*

D. B. Melrose

Research Centre for Theoretical Astrophysics, School of Physics,
University of Sydney, NSW 2006, Australia.

Abstract

The twinkling of stars is a familiar example of scintillations, due to turbulence in the Earth's atmosphere causing fluctuations in the refractive index of the air along the line of sight. Scintillations lead to time variations in the apparent position of the source, and hence to an angular broadening on integration over an observation time. Scintillations also lead to fluctuations in the intensity of the source. Pointlike astronomical radio sources such as pulsars and (the compact cores of some) quasars scintillate due to fluctuations in the electron density along the line of sight through the interstellar medium. For quasars, low-frequency (100s of MHz) variability over periods of years is a scintillation effect, as are probably more rapid (as short as an hour) intensity variations at higher radio frequencies. Unlike the twinkling of stars, which is due to weak scintillations, the scintillations of radio sources are usually strong. Important qualitative effects associated with strong scattering are multipath propagation and a clear separation into diffractive and refractive scintillations. Quasars exhibit only refractive scintillations.

Pulsars are extremely small and bright, and they vary temporally on a very short time scale, making them almost ideal sources on which to test our ideas on scintillations. Pulsars exhibit a variety of scintillation phenomena, due to both refractive and diffractive effects, the latter seen most clearly in dynamic spectra. These data are used to model the distribution of electrons through the Galaxy, to determine the distribution of pulsar velocities, and potentially to resolve the source region in a pulsar magnetosphere.

These scintillation phenomena and their interpretation in terms of the theory of strong scintillations are reviewed briefly. The generalisation of the theory to include the birefringence of the plasma (Faraday effect), and its possible implications on the interpretation of circular polarisation, are then outlined. An attempt to generalise the theory to describe scattering by a distribution of discrete scattering objects is also discussed briefly.

1. Introduction

The twinkling of stars is the most familiar scintillation phenomenon in astronomy. Twinkling is due to local inhomogeneities in one or more turbulent layers in the atmosphere, typically hundreds of metres above the ground, causing local refractive index variations, and hence distorting the wavefront of the incoming light. The direction of ray propagation is the normal to the wavefront, so that these variations cause the apparent direction of propagation, and hence the apparent position of the star, to change with time as the distorted wavefront is

* Lecture presented on the award of the Massey Prize on 29 September 1998, held during the AIP National Congress in Fremantle, Western Australia.

 10.1071/PH98076 0004-9506/99/010001$10.00

swept across the observer by the wind in the turbulent layer. The distortions include both convex and concave portions of the wavefront, and these correspond to focusing and defocusing regions, which lead to changes in the intensity of the starlight. Given the size of the inhomogeneities, $\sim$10 cm, and the speed of the wind, $100\,\mathrm{m\,s^{-1}}$, one can estimate the typical time scale for these variations, $\sim$1 ms. Conversely, the observed properties of the scintillation pattern may be used to deduce information about the properties of the turbulence. In most applications the turbulence is consistent with a Kolmogorov spectrum for density fluctuations, $\propto k^{-5/3}$, where k is the wave number of the turbulent eddies.

Scintillations of radio astronomical sources result from fluctuations in the plasma density along the line of sight to the source. This effect was first studied in detail in radio astronomy in connection with propagation through the solar wind. Radio sources that pass close to the Sun are viewed through denser regions nearer to the Sun, providing information on the inner regions of the solar wind. Some features of the radio observations of quasars and of pulsars are interpreted in terms of scintillations in the interstellar medium (ISM). Pulsars, being extremely small, extremely bright, and varying systematically on the pulse period, are almost ideal probes of the ISM, allowing construction of a model for the three-dimensional distribution of plasma through the Galaxy (e.g. Taylor and Cordes 1993).

Scintillations in the ISM can be in the regime of 'strong' scattering, whereas the twinkling of stars is usually in the regime of 'weak' scattering. The distinction between weak and strong scattering may be understood in terms of two parameters, the diffractive scale of the turbulence and the Fresnel scale. The diffractive scale, r_{diff}, is the distance across the wavefront over which the distortions cause the fluctuations in the phase to be of order a radian; a more formal definition of r_{diff} is in terms of the phase structure function, defined in $(2\cdot 9)$ below. The value of r_{diff} is determined primarily by the strength of the turbulence. The Fresnel scale, defined here as $r_{\mathrm{F}} = (L\lambda/2\pi)^{\frac{1}{2}}$, is the size of a disk at a distance L such that the phase change due to the different pathlengths from the centre to the edge of the disk is of order a radian. Weak scattering corresponds to $r_{\mathrm{diff}} \gg r_{\mathrm{F}}$, in which case only small fluctuations in phase can be observed. Strong scattering corresponds to $r_{\mathrm{diff}} \ll r_{\mathrm{F}}$, and this leads to multipath propagation. Strong scattering need not require a particularly high level of turbulence: scattering tends to be strong in radio astronomy because both L (a sizable fraction of the distance across the Galaxy) and λ are relatively large, so that $r_{\mathrm{F}}/r_{\mathrm{diff}}$ can be large even for a modest value of r_{diff}. The theory of strong scintillations was developed in the laser physics literature before its importance in radio astronomy was recognised. This theory needed only minor modifications for application to these radioastronomical applications.

The theory of strong scattering can account for a rich variety of propagation effects observed in quasars and pulsars, but there are some phenomena that require modification of the standard theory. Extreme scattering events (ESEs) (Fiedler *et al.* 1987, 1994) appear to be due to discrete structures moving across the line of sight and a different theory is required to account for such events (e.g. Clegg, Fey and Lazio 1998). Recently two of my colleagues (Walker and Wardle 1998) have proposed an interpretation of such events in terms of a new class of interstellar clouds, and this model has much wider astrophysical implications.

There are also features in the dynamic spectra of pulsars that suggest scattering by discrete structures (e.g. Rickett 1990). An attempt to generalise the theory to describe scattering by a distribution of discrete structure encounters a difficulty, explained briefly below, and a satisfactory resolution of this has yet to be achieved.

In this this paper I discuss scintillations in the ISM emphasising recent work by myself and my colleagues and students. The paper is arranged as follows. The theory of strong scintillations is reviewed briefly in Section 2, the applications of the theory to quasars is discussed in Section 3 and to pulsars in Section 4. The effect of the birefringence of the plasma is introduced in Section 5 and applied to the interpretation of polarisation data. The attempt to generalise the theory to describe scattering by a distribution of discrete objects is summarised briefly in Section 6. The results are discussed in Section 7.

2. Scintillation Theory

In the theory of strong scattering (e.g. Prokhorov *et al.* 1975; Ishimaru 1978) the effect of the fluctuations in the medium is described in terms of a hierarchy of moments of the wave amplitude. For most purposes, only two moments of the wave field are relevant: the second moment, which gives the mutual coherence or visibility function, and a fourth moment which gives the correlation function for intensity fluctuations. The turbulence is described in terms of the correlation function for the density fluctuations, which determines the correlation function for the refractive index fluctuations, and hence the correlation function for the phase fluctuations of the wave. The actual quantity used in practice is the phase structure function, $D(\mathbf{r})$, which is simply related to the phase correlation function.

The Wave Equation

The starting point for a discussion of scattering of electromagnetic waves in an isotropic, turbulent medium is the wave equation with the dielectric constant, $K(\mathbf{x})$, separated into a uniform component part, K_I, and a fluctuating part, $\delta K(\mathbf{x})$. The turbulence is assumed stationary, and the wave amplitude is assumed to vary with time as $e^{-i\omega t}$. The objective is to derive relevant moments of the wave amplitude. A perturbation method is needed to solve the equation for the wave amplitude. The simplest perturbation method is the Born approximation, which corresponds to a single scattering, but this is too severe a limitation to be useful in the theory of scintillation. The Rytov method (e.g. Chernov 1960, p. 61) involves writing the (scalar) wave amplitude in the form $E = A\exp(iS) = \exp(\psi)$, with the complex phase $\psi = \ln A + iS$, and solving by making a perturbation expansion in this phase. The Rytov method gives good agreement for propagation of light through the Earth's atmosphere for distances of order a kilometre or so, but it breaks down for propagation over longer distances.

The theory of strong scattering (e.g. Gochelashvily and Shishov 1971; Prokhorov *et al.* 1975; Uscinski 1977; Ishimaru 1978) is based on the parabolic approximation to the wave equation, in which the wave amplitude is assumed to be of the form $\mathbf{E} = \mathbf{u}e^{ikz}$, where $\mathbf{u}$ is a slowly varying function of distance z along the line of sight between the source and the observer. The first order solution of this equation is used to derive differential equations for the moments of the wave field. The most useful solutions for the second and fourth order moments may

be derived more simply using a phase averaging method (e.g. Fante 1975, 1980). An assumption common to these methods is that all the scattering is assumed to occur at a single scattering screen. An alternative method that allows for an extended region of scattering is the Feynman integral method (e.g. Tatarski and Zavorotnyi 1980), but this leads to much more cumbersome analytic expressions for the moments.

The Fresnel–Kirchhoff Integral

Let the mean ray direction be along the z axis, and let either transverse (along the x or y axes) component of the wave equation be denoted u. The wave equation then reduces to

$$\left(\nabla^2 + \frac{\omega^2}{c^2}\left[K_I + \delta K(\mathbf{x})\right]\right)(ue^{ikz}) = 0. \tag{2·1}$$

The parabolic approximation to (2·1) involves writing $\nabla^2 = \partial^2/\partial z^2 + \nabla_\perp^2$, $\nabla_\perp^2 = \partial^2/\partial x^2 + \partial^2/\partial y^2$, ignoring the second derivative with respect to z, and identifying $k^2 = (\omega^2/c^2)K_I$. Then (2·1) implies

$$\left(2ik\frac{\partial}{\partial z} + \nabla_\perp^2 + \frac{\omega^2}{c^2}\delta K\right)u = 0. \tag{2·2}$$

The solution of (2·2) in the absence of the term δK is

$$u(z,\mathbf{r}) = -\frac{ik}{2\pi(z-z')}\int d^2\mathbf{r}'\, u(z',\mathbf{r}')\, \exp\left[\frac{ik(\mathbf{r}-\mathbf{r}')^2}{2(z-z')}\right]. \tag{2·3}$$

The integral (2·3) may be interpreted as relating the amplitude at a plane $z =$ constant, which is to be identified as the image plane with $z = L$, to the amplitude at the plane $z' =$ constant, which is to be identified as the scattering screen, with $z' = 0$. The solution (2·3) then becomes the Fresnel–Kirchhoff integral

$$u(L,\mathbf{r}) = -\frac{i}{2\pi r_{\mathrm{F}}^2}\int d^2\mathbf{r}'\, u(0,\mathbf{r}')\, \exp\left[i\frac{(\mathbf{r}-\mathbf{r}')^2}{2r_{\mathrm{F}}^2}\right], \tag{2·4}$$

where the characteristic distance

$$r_{\mathrm{F}} = (L/k)^{\frac{1}{2}} \tag{2·5}$$

is the Fresnel scale.

The Phase Structure Function

In the method of Prokhorov *et al.* (1975), the differential equation (2·2) for the wave field is combined with a perturbation solution based on (2·4) to derive differential equations for the moments of the wave field, and the moments are found by solving these differential equations. A simpler approach, based on the thin screen approximation, is to regard the plane $z = L$ as a phase screen, and

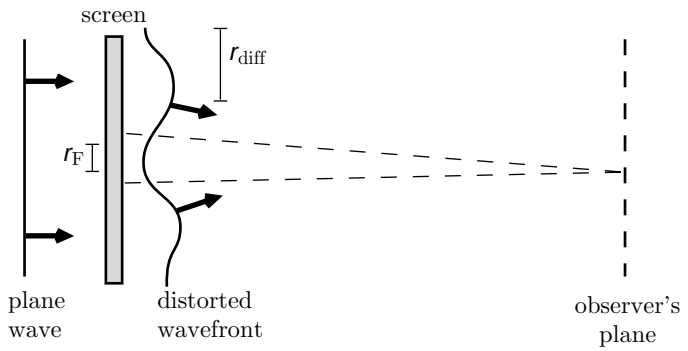

Fig. 1. The thin screen model. An incoming plane wave has phase variations imposed on it on passing through a phase screen.

to assume that the turbulence causes an incident plane wave (amplitude u_0) to have a phase fluctuation, such that it is transformed into $u_0 \exp[i\phi(\mathbf{r})]$ at the phase screen, as illustrated in Fig. 1. Then (2·4) is replaced by

$$u(z,\mathbf{r}) = -\frac{ike^{ik(z-z')}}{2\pi(z-z')} \int d^2\mathbf{r}'\, u_0 e^{i\phi(\mathbf{r})} \exp\left[\frac{ik(\mathbf{r}-\mathbf{r}')^2}{2(z-z')}\right]. \qquad (2\cdot 6)$$

The statistical average over the phase is performed assuming gaussian statistics, which gives

$$\langle e^{i[\phi(\mathbf{r})-\phi(\mathbf{r}')]}\rangle = e^{-D(\mathbf{r}-\mathbf{r}')/2}, \qquad (2\cdot 7)$$

where the phase structure function is defined by

$$D(\mathbf{r}) = \langle[\phi(\mathbf{r}') - \phi(\mathbf{r}'+\mathbf{r})]^2\rangle. \qquad (2\cdot 8)$$

The phase structure function is related to the the autocorrelation function for the fluctuations $\delta K(\mathbf{x})$, and hence to the correlation function for the density fluctuations in the turbulence. For a power law spectrum of isotropic density fluctuations one has

$$D(\mathbf{r}) = \left(\frac{r}{r_{\rm diff}}\right)^{\beta-2}, \qquad (2\cdot 9)$$

with $\beta = \frac{11}{3}$, $\beta - 2 = \frac{5}{3}$ for a Kolmogorov spectrum, and where the definition of the diffractive scale, $r_{\rm diff}$, incorporates all the normalisation constants. For some purposes it is necessary to include inner and outer scales of the turbulence, which imply cutoffs to the form (2·9) at small and large r, but many results are insensitive to these cutoffs.

The Mutual Coherence Function

The mutual coherence function is the second moment

$$I(\mathbf{r}) = \langle u(\mathbf{r}' + \mathbf{r}) u^*(\mathbf{r}') \rangle, \tag{2·10}$$

which is also the visibility function. The thin screen approximation for an incident plane wave gives

$$\frac{I(\mathbf{r})}{I(0)} = \exp[-\tfrac{1}{2} D(\mathbf{r})]. \tag{2·11}$$

The function $I(\mathbf{r})$ gives the spatial distribution of the image, and the two-dimensional spatial Fourier transform of $I(\mathbf{r})$ gives its angular distribution.

Intensity Fluctuations

The fourth order moment is defined by analogy with (2·8), with a product of four, rather than two, wave fields. The only case considered here is for the correlation in the intensities. For an incident plane wave and for a thin screen, the intensity fluctuations may be described by

$$B_I(\mathbf{r}) = \frac{\langle I(\mathbf{r}' + \mathbf{r}) I(\mathbf{r}') \rangle}{[I(0)]^2} - 1 = \int \frac{d^2\mathbf{q}}{(2\pi)^2}\, e^{-i\mathbf{q}\cdot\mathbf{r}}\, W(\mathbf{q}) - 1, \tag{2·12}$$

$$W(\mathbf{q}) = \int \mathrm{d}^2\mathbf{r} \exp(i\mathbf{q}\cdot\mathbf{r}) \exp[-D(\mathbf{r}) - D(r_{\mathrm{F}}^2 \mathbf{q}) + \tfrac{1}{2} D(\mathbf{r} + r_{\mathrm{F}}^2 \mathbf{q}) + \tfrac{1}{2} D(\mathbf{r} - r_{\mathrm{F}}^2 \mathbf{q})]\,. \tag{2·13}$$

The (integrated) power in intensity fluctuations with a wave number q may be estimated from $q^2 W(\mathbf{q})$.

Weak and Strong Scattering

The parameter

$$\xi = \frac{r_{\mathrm{F}}}{r_{\mathrm{diff}}} \tag{2·14}$$

determines whether the scattering is weak ($\xi \ll 1$) or strong ($\xi \gg 1$). The Fresnel scale, r_{F}, determines the maximum size of the coherent patch on the scattering screen when the difference in pathlength to the observer is taken into account. The diffractive scale, r_{diff}, determines the size of the 'scattering disk' over which the turbulence causes a phase change by about a radian. In weak scattering the maximum phase change due to the turbulence that an observer can detect is $[D(r_{\mathrm{F}})]^{\frac{1}{2}} \ll 1$, cf. (2·9). The exponent in (2·13) involving the $D(\mathbf{r})$ with different arguments is then always small, and may be approximated by expanding the exponential and retaining only the linear term. This leads to considerable mathematical simplification for weak scattering.

In weak scattering, the small phase change across the scattering disk causes two effects. First, there is a displacement of the image due to the slope of the wavefront, with the ray direction being normal to the wavefront. Second, the (weak) curvature of the wavefront implies a focusing (concave portion of the wavefront) or a defocusing (convex portion of the wavefront). The image sweeps across the observer's plane due to motion of the source or the scattering screen relative to the observer. This leads to temporal changes in the centroid of the image and in the intensity of the image as portions of the wavefront with different slope and curvature, respectively, sweep by. The power in intensity fluctuations on a spatial scale $\sim 1/q$ is determined by the function $q^2 W(\mathbf{q})$. As the image sweeps by, this leads to fluctuations in the intensity on a time scale $\sim 1/qv$, where v is determined by the velocities of the source and the turbulence relative to the observer.

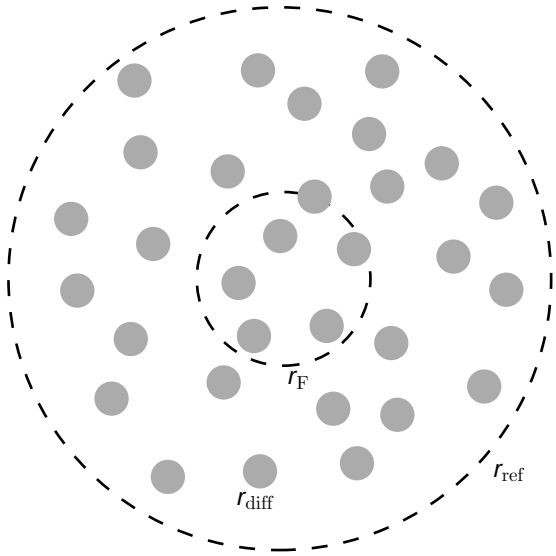

Fig. 2. Strong scattering. An observer sees many images of the source, each corresponding to a coherent patch of size $r_{\rm diff}$ in an envelope of size $r_{\rm ref}$.

The most important qualitative change as the scattering passes from weak to strong is that multipath propagation becomes important. In weak scattering there is a single coherent patch of size $\sim r_{\rm F} \ll r_{\rm diff}$. In strong scattering there are many coherent patches of size $\sim r_{\rm diff}$ inside a Fresnel radius, and one can also see coherent patches of size $\sim r_{\rm diff}$ outside a Fresnel radius, due to refraction causing the normals to the coherent patches to deviate from the direction of an undeflected ray. As illustrated in Fig. 2, the envelope of these coherent patches extends to a so-called refractive scale, $r_{\rm ref}$, with

$$r_{\rm ref} = \frac{r_{\rm F}^2}{r_{\rm diff}}. \tag{2·15}$$

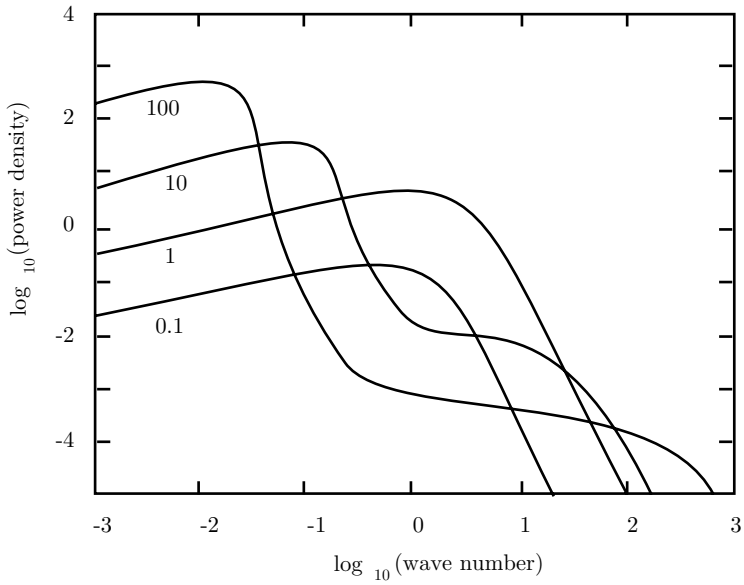

Fig. 3. Power spectrum $W(\mathbf{q})$ of intensity fluctuations for different values of the parameter ξ that describes the strength of the scattering [after Rickett (1990)]. The power observed may be estimated from $q^2W(\mathbf{q})$, and for $\xi \gg 1$ this has a diffractive peak at $q \sim 1/r_{\rm diff}$, and the factor q^2 converts the broad shoulder at larger q into a refractive peak at $q \sim 1/r_{\rm ref}$.

Intensity Fluctuations in Strong Scattering

Scintillation theory implies that the power spectrum of the intensity fluctuations, $W(\mathbf{q})$, is given by (2·13). The most important differences between weak and strong scattering may be understood by considering how the quantity $q^2W(\mathbf{q})$ changes as the parameter ξ is increased from $\xi < 1$ to $\xi > 1$, as illustrated in Fig. 3. For $\xi \ll 1$, there is a single broad peak in the intensity fluctuations at a scale $1/q \sim r_{\rm F}$, and the height of this peak rises as the strength, ξ, of the scattering increases. As ξ passes through unity, the peak bifurcates, and for $\xi \gg 1$ there are two distinct peaks, at the diffractive scale, $1/q \sim r_{\rm diff}$, and the refractive scale, $1/q \sim r_{\rm ref}$. The separation into these two scales may be understood (e.g. Tatarski and Zavorotnyi 1980) by noting that the exponent involving the functions $D(\mathbf{r})$ in (2·13) is small for $r \lesssim r_{\rm diff}$ and for $qr_{\rm F}^2 \lesssim r_{\rm diff}$ when one expands in $r/r_{\rm diff}$ and $qr_{\rm F}^2/r_{\rm diff}$, respectively. Thus, in strong scattering, the intensity fluctuations separate into diffractive and refractive scales, which are quite different and have quite different properties (e.g. Narayan 1992). In particular, diffractive scattering occurs on a time scale $t_{\rm diff} \sim r_{\rm diff}/v$ and decorrelates over a narrow frequency range, $\omega_{\rm dc} = \omega/\xi^2$, and refractive scattering occurs on a longer time scale $t_{\rm ref} \sim r_{\rm ref}/v$ over a broad frequency range. As indicated schematically in Fig. 4, as the scattering becomes strong, the scintillation index m, with

$$m^2 = \frac{\langle I^2\rangle - \langle I\rangle^2}{\langle I\rangle^2} = B_I(\mathbf{0}), \qquad (2\cdot16)$$

remains at unity for diffractive scattering, and decreases with increasing ξ for refractive scattering.

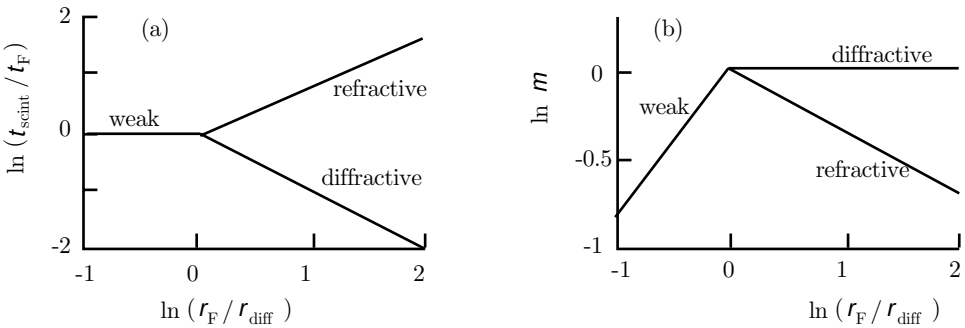

Fig. 4. Schematic plot of the variation of the scintillation time scale and the scintillation index as a function of the parameter ξ that describes the strength of the scattering [after Narayan (1992)].

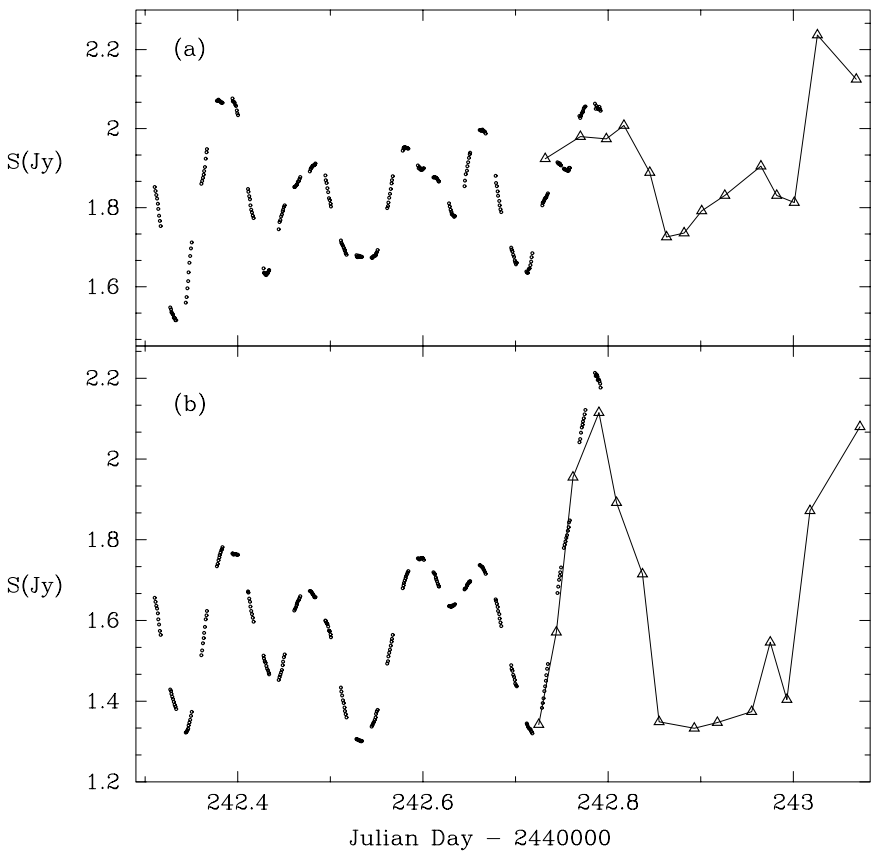

Fig. 5. Variations in the quasar PKS 0405–385: (a) at 8·6/8·4 GHz and (b) at 4·8/5·0 GHz. The circles denote data from the Australia Telescope and the triangles denote data from a South African telescope [after Kedziora-Chudczer *et al.* (1997)].

3. Flux Variations of Quasars

Flux variations of many quasars are attributed to refractive scintillations in the interstellar medium (RISS). However, the interpretation of variability is confused because of compelling evidence in some cases for RISS, and strong evidence in other cases for variability that is intrinsic to the source.

Flux Variations in Quasars

Some quasars have long been known to vary at high frequencies ($\gg 1\,\mathrm{GHz}$), typically involving outbursts in which a new compact component appears and evolves by expanding and ultimately fading into the overall spectrum of the quasar (e.g. Kellerman and Pauliny-Toth 1981). It was a surprise when it was recognised that some quasars also exhibit low-frequency ($< 1\,\mathrm{GHz}$) variability (LFV) on a time scale of years (Hunstead 1972). If such variations were intrinsic to the source, they would imply brightness temperatures in excess of the limit of $10^{12}\,\mathrm{K}$ set by the inverse Compton catastrophe for a synchrotron source (Kellerman and Pauliny-Toth 1969; Jones and Burbidge 1973).

Subsequently more rapid variations were found, and these are referred to as flickering and intra-day variability (IDV) (e.g. Rickett 1990). Flickering involves flux variations of a few per cent on a time scale of several days. IDV was reviewed by Wagner and Witzel (1995), who argued that it is intrinsic to the source. Their argument is based primarily on apparently correlated variations at radio and optical wavelengths, and the latter certainly cannot be due to RISS.

An extreme example of IDV was reported by Kedziora-Chudczer *et al.* (1997) for observations with the Australia Telescope of the source PKS 0405–385, cf. Fig. 5. This source varied rapidly, with a time scale of an hour or so, but this extreme activity lasted only several weeks. A notable feature of the intensity fluctuations is that they do not increase with decreasing frequency, as one would expect for weak scintillations. Also notable is the change in the linear and circular polarisations as the source scintillates. The Australia Telescope is well designed to measure circular polarisation accurately, and the changes in circular polarisation have no standard explanation.

Application of RISS to Quasars

The interpretation of low-frequency flux variability in terms of RISS was proposed by Shapirovskaya (1978), but did not become widely accepted until somewhat later (e.g. Rickett, Coles and Bourgois 1984). This interpretation overcomes the difficulty with brightness temperature $> 10^{12}\,\mathrm{K}$ and allows the synchrotron hypothesis to be retained for quasars that exhibit LFV.

The interpretation of flickering and of IDV is not as clear as for LFV. The interpretation is obscured by there being strong evidence for both RISS and for intrinsic variability, and it is thought that both contribute to the variations of different sources. The sources for which the variations are probably intrinsic tend to be sources in which there is evidence for relativistic jets, with the strongest such evidence from apparent superluminal expansion (e.g. Blandford 1990). In a model in which the transverse separation is between an oncoming source

(embedded in a jet) and a stationary core component, the apparent transverse expansion speed is

$$\beta_{\rm obs} = \frac{\beta \sin\theta}{1 - \beta\cos\theta}, \qquad (3\cdot 1)$$

where the jet has speed βc and Lorentz factor $\gamma = 1/(1-\beta^2)^{\frac{1}{2}}$ and is viewed at an angle θ. The maximum transverse expansion speed is for $\cos\theta = \beta$, when one has $\beta_{\rm obs} = \gamma\beta$, which is superluminal for $\beta > 1/\sqrt{2}$ or $\gamma > \sqrt{2}$.

For a relativistic jet, the observed brightness temperature is higher than the brightness temperature inferred from the variability by a Doppler boost factor $\mathcal{D}^3$, with $\mathcal{D} = [\gamma(1-\beta\cos\theta)]^{-1}$. By postulating a sufficiently large $\mathcal{D}$, any observed brightness temperature can be made consistent with $T_b < 10^{12}\,$K in the rest frame of the jet. There is evidence for values of $\gamma \sim 10$ from superluminal motions, but the values $\gamma > 10^3$ required to explain IDV by this mechanism are considered implausible.

Kedziora-Chudczer *et al.* (1997) argued that the IDV in the source PKS 0405–385 is due to RISS. The component of the source causing the variability, presumably associated with an outburst in the source, must be very small. The small size implies a high brightness temperature, estimated to be $T_b > 5\times 10^{14}\,$K. Doppler boosting is still required for the inverse Compton limit not to be violated, and in this case the boost factor is only a single power of $\mathcal{D}$. Hence an extreme value, $\gamma \gtrsim 10^3$, for the Lorentz factor of the bulk flow is still required.

Walker (1998) discussed the application of RISS to extragalactic sources in detail using a model for the distribution of plasma in the interstellar medium developed by Taylor and Cordes (1993) from pulsar data. He pointed out that the condition $\xi = 1$, with $\xi \propto \omega^{-1\cdot 7}$, defines a transition frequency between weak and strong scattering. This frequency is in the range over which observations of extragalactic sources are usually made: it is $\sim 5\,$GHz for sources at high Galactic latitudes, and at higher frequencies for sources near the Galactic plane. An important qualitative point is that for sources at high Galactic latitudes varying due to RISS one predicts that the scintillation index should have a maximum at $\sim 5\,$GHz, and should decrease towards both higher frequencies (as the scattering becomes weak) and lower frequencies, in accord with Fig. 4 for strong scattering. The fact that PKS 0405–385 showed such a dependence supports the interpretation in terms of RISS.

In summary, it appears that variability of quasars can be explained in terms of one of three effects, RISS, intrinsic variability or Doppler boosting. However, all three effects are required for different sources. Moreover, in some cases the parameters (notably the Lorentz factor of the jet) required are rather extreme, and it is desirable to reconsider the assumptions involved in estimating the inverse Compton limit to see whether it can be relaxed (to allow T_b somewhat greater than $10^{12}\,$K) without implying catastrophic inverse Compton losses.

4. Scintillations of Pulsars

Pulsars are extremely small (a few 100 m) and extremely bright ($T_b \gtrsim 10^{25}\,$K) and vary in a characteristic, repeatable way on a very short time scale ($\sim 10^{-1\pm 2}\,$s). As such they are almost ideal examples to test ideas on scintillations. Unlike quasars,

whose angular sizes are too large to allow DISS, pulsars exhibit scintillation phenomena including effects due to both RISS and DISS.

Propagation Phenomena Observed in Pulsars

Propagation phenomena observed in pulsars include dispersion of pulses, secular variations in pulse to pulse height, pulse broadening, and timing noise. Dispersion results from the frequency dependence of the refractive index, $n(\omega) \approx 1 - \omega_p^2/2\omega^2$. The group speed is $cn(\omega)$, and hence the propagation speed decreases as the frequency decreases. As a consequence the lower frequencies arrive later than the higher frequencies. Observation of this effect allows one to determine an observational parameter which is the integral along the line of sight of ω_p^2. The quantity actually estimated is the dispersion measure, DM, defined by

$$\mathrm{DM} = \int ds\, n_e. \tag{4·1}$$

With an appropriate estimate of the plasma density along the line of sight, DM may be used as a measure of the distance to the pulsar. Any independent information on the distances to pulsars allows refinement of the model for the plasma distribution in the ISM, and so of the relation between DM and distance.

As with quasars the first evidence for RISS in pulsars was unexpected. Sieber (1982) noted that secular variations in different pulsars correlated with the positions, suggesting a propagation effect, for which RISS provided a natural explanation (Rickett, Coles and Bourgois 1984). Observations of RISS enable one to determine a parameter related to the strength of the scattering. In an analogous way to the definition of DM, a scattering measure, $\mathrm{SM} = \int ds\, C_N^2$, is defined, where C_N^2 is the constant of proportionality in the power law spectrum of density fluctuations, $\propto C_N^2 q^{-\beta}$. Both DM and SM, as well as other data, are used in constructing models for the distribution of plasma in the ISM throughout the Galaxy (e.g. Taylor and Cordes 1993).

Pulse broadening is another propagation effect, the theory for which (e.g. Lee and Jokipii 1975) implies a characteristic profile, as illustrated in Fig. 6. Observed pulse profiles of a number of pulsars are consistent with this profile suggesting that such pulse broadening is a propagation effect rather than being intrinsic to the source (e.g. Rickett 1977).

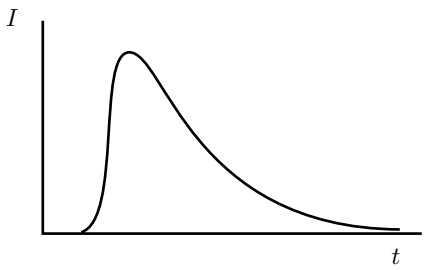

Fig. 6. Characteristic pulse shape (intensity and a function of time) imposed on an impulse by propagation through a turbulent plasma [after Lee and Jokipii (1975)].

Scintillation Velocities

The clearest demonstration of DISS in pulsars is shown by dynamic spectra, as illustrated in Fig. 7. The dynamic spectra often exhibit a highly structured pattern characteristic of interference fringes. The bright patches in the frequency–time plane are called scintles, which are interpreted in terms of the characteristic time, $t_{\rm diff}$, and (decorrelation) bandwidth, $\omega_{\rm dc} \sim \omega/\xi^2$, expected for DISS. The observed pattern of scintles is quite variable from pulsar to pulsar, and can also be quite variable for a given pulsar from one epoch to another. The scintillation pattern can include drifting bands, criss–cross patterns and periodic patterns.

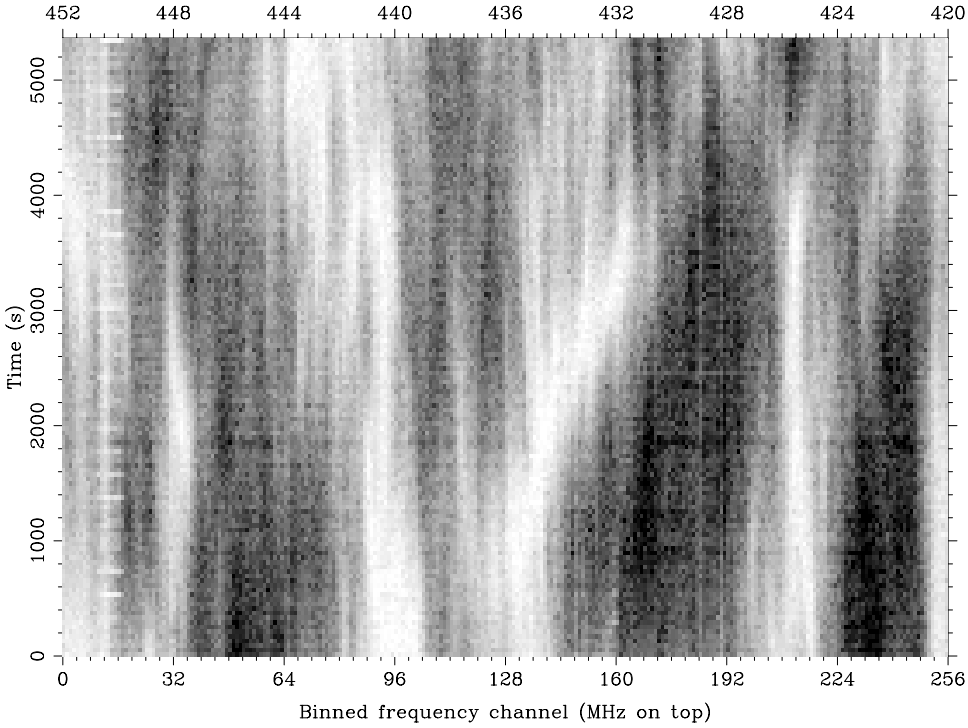

Fig. 7. Example of a dynamic spectrum of a pulsar (PSR 1456–6843) showing diffractive scintillations [after Johnston, Nicastro and Koribalski (1998)].

The scintillation pattern may be used to estimate the transverse velocity of pulsars (Cordes 1986). The idea is based on the slope of scintles in the frequency–time plane depending on the relative velocity of the pulsar to the scattering screen and the observer, and hence the pattern may be used to estimate this velocity. When combined with other methods for measuring the transverse velocity (measuring proper motions through radio interferometry at different epochs or timing observations over many years) this method provides a statistical distribution of transverse velocities for a large number of pulsars (Gupta 1995; Johnston, Nicastro and Koribalski 1998). The speeds of pulsars are unexpectedly high, with a mean of several $100\,{\rm km\,s^{-1}}$. This implies that neutron stars are given a large kick at their birth in a supernova explosion, and at present there is no entirely satisfactory explanation for this.

Resolving the Pulsar Magnetosphere

In principle, scintillations may be used to resolve an otherwise unresolvable source. Qualititatively, this may be understood by regarding the largest scale density inhomogeneities associated with the turbulence as acting like large lenses. Although the inhomogeneities are far from ideal lenses, a statistical distribution of such inhomogeneities can allow one, in principle, to deduce similar information that one could obtain with an ideal lens. However, existing attempts to resolve the source region in a pulsar magnetosphere (Wolszczan and Cordes 1987; Gwinn *et al.* 1997) have yet to lead to unambiguously positive results. Nevertheless, the principle seems clear (e.g. Cornwall and Narayan 1993), and it is anticipated that some convincing evidence on the structure of pulsar source regions will ultimately be deduced using scintillations.

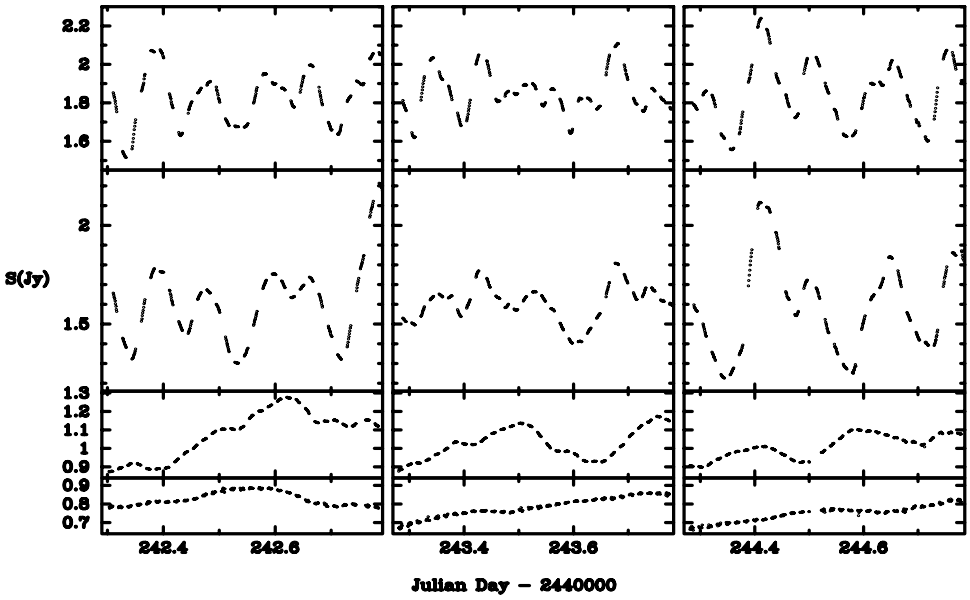

Fig. 8. Variations in the quasar PKS 0405–385 showing the linear and circular polarisations [after Kedziora-Chudczer *et al.* (1997)].

5. Circular Polarisation of Extragalactic Sources

Circular polarisation is unmeasurably small for most extragalactic radio sources. However, there is subclass of (flat-spectrum) sources for which circular polarisation is detectable, e.g. Fig. 8, and for which there is no satisfactory explanation (e.g. Roberts *et al.* 1975). Synchrotron theory implies a small circular polarisation, but with a characteristic frequency dependence which is not consistent with the data. The observed circular polarisation is also variable, and this is consistent with it being a scintillation effect. The following model for circular polarisation due to a propagation effect is being developed in collaboration with J.-P. Macquart, and appears here in preliminary form for the first time.

Scintillations in a Birefringent Plasma

The ISM is birefringent due to the interstellar magnetic field. The natural modes are circularly polarised (the ellipticity is extremely small). Scintillation theory was generalised to take account of the birefringence by Kukushkin and Ol'yak (1990, 1991) and Melrose (1993*a*, 1993*b*). A somewhat different (but essentially equivalent) form of the generalisation is summarised in Appendix A.

Stochastic Faraday Rotation

Before discussing circular polarisation, it is relevant to discuss the effect of the birefringence on the linear polarisation. As in the case of the effects of dispersion, there is a systematic effect due to the homogeneous component of the ISM. This leads to Faraday rotation, which is a steady rotation of the plane of linear polarisation due to the right- and left-hand polarisation components getting systematically out of phase due to the small difference in refractive index. As with dispersion and the DM, the characteristic frequency dependence of Faraday rotation allows the measurement of a parameter, called the rotation measure RM, which is proportional to the integral along the line of sight of the electron number density times the line of sight component of the magnetic field,

$$\mathrm{RM} = \int d\mathbf{s} \cdot \mathbf{B}\, n_e, \tag{5·1}$$

where the $d\mathbf{s}$ denotes an infinitesimal displacement along the ray path.

It is conventional to express the intensity for polarised radiation in terms of the Stokes parameters, I, Q, U, V. In the theory outlined in Appendix A, the specific intensities $I_{\sigma\sigma'}$ in the two orthogonally polarised natural modes (denoted $\sigma, \sigma' = \pm$) appear, and in the present case the natural modes are circularly polarised. For circularly polarised natural modes (denoted $\sigma, \sigma' = r$ or l) one has

$$I = \tfrac{1}{2}(I_{rr} + I_{ll}), \qquad Q = \tfrac{1}{2}(I_{rl} + I_{lr}), \qquad U = i\tfrac{1}{2}(I_{rl} - I_{lr}), \qquad V = \tfrac{1}{2}(I_{rr} - I_{ll}),$$
$$I_{rr} = I + V, \qquad I_{ll} = I - V, \qquad I_{rl} = Q - iU, \qquad I_{lr} = Q + iU. \tag{5·2}$$

The relations (5·2) apply to the visibilities, e.g. $I(\mathbf{r})$ with $\mathbf{r}$ nonzero, as well as to the Stokes parameters themselves, that is, for $\mathbf{r} = 0$. As noted following equation (A·10) in Appendix A, Faraday rotation remains in the theory of scintillation in a birefringent plasma when the turbulence is absent, and then it affects only the Stokes parameters Q and U, which describe the linear polarisation.

Turbulence in the ISM causes a random component of Faraday rotation. This may be described by the fourth order moment of the wave amplitude, cf. equation (A·14) of Appendix A. The resulting equations for $\langle Q^2 \rangle$, $\langle U^2 \rangle$, $\langle QU \rangle$ may be derived using a much simpler model in which the Faraday angle (through which the plane of polarisation rotates) has a random component that obeys gaussian statistics (Burn 1966). Thus this effect is equivalent to stochastic Faraday rotation, which can lead to a form of depolarisation (Burn 1966). This type of depolarisation has a characteristic feature ($\langle Q \rangle$ and $\langle U \rangle$ decrease with $\langle Q^2 + U^2 \rangle$ remaining constant) that allows one to distinguish it from other types

of depolarisation (Melrose and Macquart 1998). Observation of this effect would provide a further measure of quantities along the line of sight; in this case the parameter is effectively the variance of RM (Melrose and Macquart 1998).

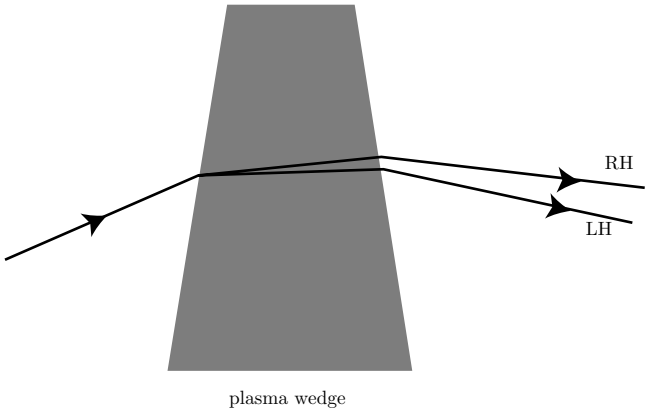

Fig. 9. Model for a Faraday wedge. An incident unpolarised ray splits into two rays in the different modes inside the plasma wedge, and these emerge with an angular separation between them.

The Faraday Wedge

The fourth order moment, given by equation (A·14) of Appendix A, implies that $\langle V^2 \rangle$ is nonzero. Thus, even for unpolarised incident radiation, the scattered radiation is partially circularly polarised in general. This effect is not due to imposition of a specific handedness because the mean circular polarisation remains zero, $\langle V \rangle = 0$.

The expression for $\langle V^2 \rangle$ implied by (A·14) is equivalent to an expression derived using a simple model for refraction in a Faraday wedge, as illustrated in Fig. 9. An essential requirement is a gradient in RM perpendicular to the line of sight. Such a wedge acts like a birefringent crystal in separating the rays corresponding to the two modes. This separation may be treated using geometric optics as follows.

The equation for a ray in mode σ is

$$\frac{d(n_\sigma \, \kappa)}{dz} = \frac{\partial n_\sigma}{\partial \mathbf{r}}, \tag{5·3}$$

where κ is the ray direction, which is assumed to be very nearly along the mean ray direction, which is the z axis. In a weakly anisotropic medium, as is the case here, one may write

$$n_\sigma = n + \sigma \Delta n, \tag{5·4}$$

with $\sigma = \pm 1$ denoting the two modes. In terms of the magnetoionic parameters, assuming both $X = \omega_p^2/\omega^2 \ll 1$ and $Y = \Omega_e/\omega \ll 1$, where $\Omega_e = eB/m$ is the electron cyclotron frequency, one has $n = 1 - \frac{1}{2}X$, $\Delta n = \frac{1}{2}XY$. In the simplest

model the inhomogeneity is only in the plasma density, so that X but not Y is a function of position. The change, $\delta\kappa_\sigma$, across a wedge of thickness δz is

$$\delta\kappa_\sigma = \delta\kappa + \tfrac{1}{2}\sigma\delta\Delta\kappa, \qquad \delta\kappa = \frac{1}{n}\int_0^{\delta z} dz\,\frac{\partial n}{\partial \mathbf{r}},$$

$$\delta\Delta\kappa = -\frac{\Delta n}{n}\,\delta\kappa + \frac{1}{n}\int_0^{\delta z} dz\,\frac{\partial \Delta n}{\partial \mathbf{r}}. \tag{5·5}$$

If the gradient is confined to say the x-z plane, with $\Delta\psi$ the angle between $\Delta\kappa$ and the x axis, then (5·5) implies the different angles, $\Delta\psi_\sigma$, through which the two modes are refracted:

$$\delta\psi_\sigma = \delta\psi + \tfrac{1}{2}\sigma\delta\Delta\psi, \qquad \delta\psi = \frac{1}{n}\int_0^{\delta z} dz\,\frac{\partial n}{\partial x},$$

$$\delta\Delta\psi = -\frac{\Delta n}{n}\,\delta\psi + \frac{1}{n}\int_0^{\delta z} dz\,\frac{\partial \Delta n}{\partial x}. \tag{5·6}$$

Thus, if the wedge is a distance L from the observer, the displacement of the centres of the images in the two modes on the observer's plane is $L\Delta\alpha$ with

$$\Delta\alpha = -\frac{\Delta n}{n}\int_0^{\delta z} dz\,\frac{\partial n}{\partial x} + \int_0^{\delta z} dz\,\frac{\partial \Delta n}{\partial x}. \tag{5·7}$$

The circular polarisation arises in this model because the rays corresponding to the opposite circular polarisations emerge from the Faraday wedge propagating in slightly different directions. When viewed from a sufficient distance, the small separation between the rays can lead to two images, in right- and left-hand polarisations, which do not overlap exactly. If the displacement between the centres of these images exceeds their size, then in strong scattering one has many overlapping images half of which have right-hand polarisation and half of which have left-hand polarisation. Even if the images partially overlap, the opposite edges must be circular polarised. For such a model, $\langle V^2\rangle$ is nonzero and its value depends on the number of images (determined statistically by the parameter ξ) and the degree of separation of the right- and left-hand components in each image.

Application to the Vela Pulsar

Numerical estimates for the foregoing effect have been made by J.-P. Macquart (private communication) for a Faraday wedge inferred from data on the Vela pulsar. Hamilton, Hall and Costa (1985) reported a temporal change in the RM of $d\mathrm{RM}/dt = 0{\cdot}73\,\mathrm{rad\,m^{-2}\,yr^{-1}}$ for the Vela pulsar. This was interpreted as a magnetised interstellar cloud crossing the line of sight, and we identify this as the Faraday wedge. The temporal change translates into a spatial gradient in $|\mathrm{grad\ RM}| = |d\mathrm{RM}/dt|/v$, where v is the speed of the wedge transverse to the line of sight. The speed of the wedge is uncertain, but probably no less than 100 km

s^{-1}, which is the scintillation speed for Vela, but possibly as high as 500 km s^{-1} (Hamilton, Hall and Costa 1985). The magnetic field in the wedge is assumed at a typical value for the ISM, $B = 0\cdot3\,\mathrm{nT}$. The size of the scattering disk for the Vela pulsar was estimated by Gwinn *et al.* (1997) to be ∼1 AU at ∼2·3 GHz.

Consider whether this Faraday wedge can account for an observed root mean square (rms) value of circular polarisation for the Vela pulsar of $\sim10^{-3}$ at 660 MHz. If we assume the scaling implied by a Kolmogorov spectrum of density inhomogeneities, the scattering disk has a size $r_{\mathrm{ref}} \sim 15\,\mathrm{AU}$ at 660 MHz. The change in the Faraday angle across the scattering disk is $\phi_{\mathrm{F}} = \alpha\Delta\phi = \alpha[D(r_{\mathrm{ref}})]^{\frac{1}{2}}$, with $\alpha = eB/m\omega$, and where $\Delta\phi$ is the phase change due to the density gradient in the wedge. With these numbers the foregoing theory implies an rms value for V/I of $0\cdot28$ for $v = 100\,\mathrm{km\,s^{-1}}$ and $0\cdot07$ for $v = 500\,\mathrm{km\,s^{-1}}$. This is of the correct order of magnitude, and suggests that the mechanism may provide a viable explanation for the observed circular polarisation of the Vela pulsar. However, the circular polarisation of the Vela pulsar is consistently right-hand and apparently stronger at higher frequencies (Han *et al.* 1998), and this does not appear to be consistent with the Faraday wedge interpretation. The suggestion that this mechanism might account for the circular polarisation of a much wider class of sources is currently being explored.

6. Scattering by a Distribution of Discrete Objects

The observational evidence for scattering by discrete objects in the ISM is strongest for ESEs (Fiedler *et al.* 1987, 1994), and these require a specific type of large-scale discrete structure to account for them (e.g. Walker and Wardle 1998). There are other less spectacular features observed in the dynamic spectra of pulsars that suggest that discrete structures contribute to scattering in the ISM (Rickett 1990). This raises the question as to how the theory for scattering needs to be generalised to include scattering by discrete structures. Such a generalisation has been attempted by the author and J.-P. Macquart and this is described briefly here. A difficulty is encountered, and it appears that this can be overcome only by relaxing the thin screen approximation.

As an aside, it is appropriate to note one general feature of a theory for scattering by a distribution of discrete objects. This is that the power spectrum of the intensity fluctuations can be determined by two effects in a model for discrete scatterers, and these two dependences apply in different ranges of wave number. Given a distribution of scatterers of different sizes, the power spectrum is determined primarily by the distribution of the sizes of the scattering objects. However, at sufficiently high wave numbers (small scales) the structure of the individual objects can be resolved. For example, if the discrete objects have sharp edges, then the power spectrum at high q is determined by these edges, and this implies a $\beta = 4$ spectrum in (2·9) and thence in (2·13). Thus, in principle the high-q dependence of the scintillation patterns should show the effects of discrete structures if they are present.

Phase Correlation Function for Scattering by N Fixed Objects

Consider scattering of a plane wave propagating in the z direction by N discrete objects. In the paraxial approximation the ith object causes a phase change $\Delta\phi_i(\mathbf{r})$. Let the ith object be centred at $\mathbf{r} = \mathbf{r}_i$, and assume it to cause

a phase change $\Delta\phi_i f_i(\mathbf{r}-\mathbf{r}_i)$, where $\Delta\phi_i$ is a constant and $f_i(\mathbf{r})$ characterises the profile of the ith object. For simplicity we assume here the N objects to be identical (an assumption which is readily relaxed, cf. Appendix B), with $\Delta\phi_i = \Delta\phi_0$ and $f_i(\mathbf{r}) = f(\mathbf{r})$.

The net effect of the N objects is to cause a phase change

$$\Delta\phi(\mathbf{r}) = \sum_{i=1}^{N} \Delta\phi_i f_i(\mathbf{r}-\mathbf{r}_i). \tag{6·1}$$

The phase correlation function is

$$C(\mathbf{r}) = \frac{1}{A}\int d^2\mathbf{r}'\,\Delta\phi(\mathbf{r}')\Delta\phi(\mathbf{r}'+\mathbf{r}), \tag{6·2}$$

where A is a normalisation area. The phase structure function is

$$D(\mathbf{r}) = 2[C(\mathbf{0}) - C(\mathbf{r})]. \tag{6·3}$$

The Fourier transform of $C(\mathbf{r})$ is

$$\tilde{C}(\mathbf{q}) = \sum_{i,j=1}^{N} \frac{\Delta\phi_i\Delta\phi_j}{A}\,\tilde{f}_i(\mathbf{q})\tilde{f}_j^*(\mathbf{q})\,e^{-i\mathbf{q}\cdot(\mathbf{r}_i-\mathbf{r}_j)}, \tag{6·4}$$

which is convenient for performing the averages over the locations of the objects. The sum in (6·4) may be separated into the diagonal terms, $i = j$, which are independent of the locations, $\mathbf{r}_i$, of the scatterers, and the off-diagonal terms, $i \neq j$, which depend only on the separations, $\mathbf{r}_i - \mathbf{r}_j$, between each pair of scatterers.

There is an accepted physical separation into 'incoherent scattering' in which interference between different scatterers is zero or is neglected, and 'coherent scattering' which is due to interference between the effects of the different scatterers. The incoherent and coherent scattering terms correspond here to the diagonal and off-diagonal terms, respectively. On physical grounds we expect the relative importance of incoherent and coherent scattering to depend on the number of objects that overlap when projected onto the scattering screen, that is, on the number of objects through which a particular ray passes. The packing of the objects may be said to be *dense* if a given ray passes through many objects, and *sparse* if a ray has a small probability of passing through an object. Coherent scattering should dominate in the limit of dense packing. In the continuum limit, corresponding to a very large number of discrete objects, dense packing should dominate completely.

Statistical Average of the Locations of the Scatterers

However, we encounter a difficulty in formulating a theory based on coherent scattering: in the simplest case the effect averages to zero. Specifically, the average over the distribution of locations gives zero for coherent scattering for a statistically uniform distribution of scatterers (e.g. Lax 1951). It follows that

some assumption in the foregoing model needs to be relaxed to obtain a nonzero result for coherent scattering.

Let us reconsider the assumption of a spatially uniform (across the scattering screen) distribution of scatterers. A nonzero result is obtained for a nonuniform distribution, which may be described by the two-point correlation function, $g(\mathbf{r})$. For example, in systems where there is a nonuniformity due to internal forces, such as in a self-gravitating system (e.g. Peebles 1993) or a thermal plasma (e.g. Klimontovich 1967, p. 125), $g(\mathbf{r})$ may be calculated within the framework of the specific model. In another type of application, in which a discrete model is used to simulate a turbulent spectrum with a given density autocorrelation function, $C_n(\mathbf{r})$, the two-point correlation function is to be chosen to satisfy $g(\mathbf{r}) = C_n(\mathbf{r})/C_n(\mathbf{0}) - 1$ (Keller 1964). However, neither of these ways of determining $g(\mathbf{r})$ is relevant in the application here, and there seems to be no reason to have $g(\mathbf{r}) \neq 0$ in the present context.

Another assumption that needs to be reconsidered is that of a single scattering screen. This is equivalent to assuming that all the scattering objects are in a single plane. The separation of two objects along the line of sight implies that the wavefront changes its shape in propagating from one object to the next, and this effect is ignored in assuming a single scattering screen. Thus the next step in this investigation is to relax the assumption of a single scattering screen and to take account of the locations of the scattering objects in three dimensions explicitly.

7. Conclusions

The most notable features of the theory of strong scintillations are multipath propagation and intensity fluctuations splitting into two well separated 'diffractive' and 'refractive' length scales and associated time scales.

The theory applied to scattering in the interstellar medium provides satisfactory explanations for many radioastronomical phenomena in quasars and pulsars. For quasars it provides the accepted interpretation for low-frequency variability on a time scale of years, and it can account for the more rapid variations at higher frequencies known as flickering and intra-day variability. Even for the most extreme example known (Kedziora-Chudczer *et al.* 1997) the theory of strong scattering is favoured, provided a suggested correlation between radio and optical variations (Wagner and Witzel 1995) is ignored. For quasars only refractive interstellar scattering (RISS) can be observed because, even in the most extreme case, the angular size of the source is too large for diffractive scattering (DISS) to be observed. For pulsars, there is a rich variety of phenomena due to propagation effects, including pulse dispersion, pulse broadening, some pulse-to-pulse variations, some timing noise and image wander. Diffractive effects are most obvious in the variety of fringe patterns observed in dynamic spectra, which are used to infer the transverse velocity of the pulsar.

Two aspects of the theory of scintillations that are currently under investigation are a possible explanation of circular polarisation for some sources, and the possible role of discrete objects in the scattering. As discussed in Section 6, it is possible in principle to account for variable circular polarisation of the order of magnitude observed, and which changes on the appropriate (refractive) time scale. Although this result is a preliminary one, the suggestion that circular

polarisation in sources that otherwise exhibit RISS is quite favourable. The attempt to formulate a model for scattering by a distribution of discrete objects encounters a difficulty that has yet to be overcome. However, it is already apparent that the discrete model is useful in itself, and the procedure by which it may be used to simulate scattering by a turbulent field with given spectrum is well established.

Acknowledgments

I thank my students and colleagues for their assistance in preparing this paper, in particular, Lucyna Kedziora-Chudczer, Jean-Pierre Macquart, Simon Johnston, Mark Walker and Mark Wardle. I also thank the referee, Dick Manchester, for helpful comments.

References

Blandford, R. D. 1990 Physical processes in active galactic nuclei in R. D. Blandford, H. Netzer and L. Woltjer (eds) *Active Galactic Nuclei*, Springer (Berlin), pp. 161–275

Burn, B. J. 1966 On the depolarisation of discrete radio sources by Faraday rotation *Mon. Not. R. Astron. Soc.* **133**, 67–83

Chernov, L. A. 1960 Wave Propagation in a Random Medium Dover (New York)

Clegg, A. W., Fey, A. L., and Lazio, T. J. W. 1998 The gaussian plasma lens in astrophysics: refraction *Astrophys. J.* **496**, 253–66

Cordes, J. M. 1986 Space velocities of radio pulsars from interstellar scintillations *Astrophys. J.* **311**, 183–96

Cornwall, T. J., and Narayan, R. 1993 Imaging with ultra-resolution in the presence of strong scattering *Astrophys. J.* **408**, L69–72

Fante, R. L. 1975 Electromagnetic beam propagation in turbulent media *Proc. IEEE* **63**, 1669–92

Fante, R. L. 1980 Electromagnetic beam propagation in turbulent media: an update *Proc. IEEE* **63**, 1424–43

Fiedler, R., Dennison, B., Johnston, K. J., and Hewish, A. 1987 Extreme scattering events caused by compact structures in the interstellar medium *Nature* **326**, 675–8

Fiedler, R., Dennison, B., Johnston, K. J., Waltman, E. B., and Simon, R. S. 1994 A summary of extreme scattering events and a descriptive model *Nature* **430**, 581–94

Gochelashvily, K. S., and Shishov, V. I. 1971 Focused irradiance fluctuations beyond a layer turbulent atmosphere *Optica Acta* **19**, 327–32

Gupta, Y. 1995 On the correlation between proper-motion velocities and scintillation velocities of radio pulsars *Astrophys. J.* **451**, 717–23

Gwinn, C. R., Ojeda, M. J., Britton, M. C., Reynolds, J. E., Jauncey, D. L., King, E. A., McCulloch, P. M., Lovell, J. E. J., Flanagan, C. S., Smits, D. P., Preston, R. A., and Jones, D. L. 1997 Size of the Vela pulsar's radio emission region: 500 kilometers *Astrophys. J.* **483**, L53–6

Hamilton, P. A., Hall, P. J., and Costa, M. E. 1985 Changing parameters along the path to the Vela pulsar *Mon. Not. R. Astron. Soc.* **214**, 5_P–8_P

Han, J. L., Manchester, R. N., Xu, R. X., and Qiao, G. J. 1998 Circular polarisation in pulsar integrated profiles *Mon. Not. R. Astron. Soc.* **300**, 373–87

Hunstead, R. W. 1972 Four variable radio sources at 408 MHz *Astrophys. Lett.* **12**, 193–200

Ishimaru, A. 1978 Wave Propagation and Scattering in Random Media Academic Press (New York)

Johnston, S., Nicastro, L., and Koribalski, B. 1998 Scintillation parameters for 49 pulsars *Mon. Not. R. Astron. Soc.* **297**, 108–16

Jones, T. W., and Burbidge, G. R. 1973 On the problem of explaining decimeter flux variations in 3C 454. 3 and other extragalactic sources *Astrophys. J.* **186**, 791–9

Kedziora-Chudczer, L., Jauncey, D. L., Wieringa, M. H., Walker, M. A., and Nicolson, G. D. 1997 PKS 0405–385: the smallest radio quasar? *Astrophys. J.* **490**, L9–12

Keller, J. B. 1964 Stochastic equation and wave propagation in random media *Proc. Symp, Applied Math.* Vol. 16, Amer. Math. Soc. (Providence, R.I.), pp. 145–70

Kellermann, K. I., and Pauliny-Toth, I. I. K. 1969 The spectra of opaque radio sources *Astrophys. J.* **155**, L71–8

Kellermann, K. I., and Pauliny-Toth, I. I. K. 1981 Compact radio sources *Ann. Rev. Astron. Astrophys.* **19** 373–410

Klimontovich, Yu. L. 1967 The Statistical Theory of Non-equilibrium Processes in a Plasma Pergamon Press, Oxford

Kukushkin, A. V., and Ol'yak, M. R. 1990 Transfer of a polarisation of radio-frequency radiation in a randomly inhomogeneous, magnetically active plasma *Radiophys. Quantum Electron.* **33**, 1002–8; *Radiofiz.* **33**, 1361–9

Kukushkin, A. V., and Ol'yak, M. R. 1991 Polarisation fluctuation in the radiation from cosmic sources due to scattering in a random inhomogeneous magnetoactive active plasma *Radiophys. Quantum Electron.* **34**, 612–18; *Radiofiz.* **34**, 738–47

Lax, M. 1951 Multiple scattering of waves *Rev. Mod. Phys.* **23**, 287–310

Lee, L. C., and Jokipii, J. R. 1975 Strong scintillations in astrophysics. II. A theory of temporal broadening of pulses *Astrophys. J.* **201**, 532–43

Melrose, D. B. 1993*a* Scintillations in a magnetised plasma 1. The mutual coherence function *J. Plasma Phys.* **50**, 267–81

Melrose, D. B. 1993*b* Scintillations in a magnetised plasma 2. The fourth order moment *J. Plasma Phys.* **50**, 283–91

Melrose, D. B., and Macquart, J.-P. 1998 Stochastic Faraday rotation *Astrophys. J.* **505**, 921–7

Narayan, R. 1992 The physics of pulsar scintillation *Phil. Trans. R. Soc. Lond.* A **341**, 151–65

Peebles, P. J. E. 1993 Principles of Physical Cosmology Princeton University Press

Prokhorov, A. M., Bunkin, F. V., Gochelashvily, K. S., and Shishov, V. I. 1975 Laser irradiance propagation in turbulent media *Proc. IEEE* **63**, 790–811

Rickett, B. J. 1977 Interstellar scattering and scintillation of radio waves *Ann. Rev. Astron. Astrophys.* **15**, 479–504

Rickett, B. J. 1990 Radio propagation through the turbulent interstellar medium *Ann. Rev. Astron. Astrophys.* **28**, 561–605

Rickett, B. J., Coles, W. A., and Bourgois, G. 1984 Slow scintillations in the interstellar medium *Astron. Astrophys.* **134**, 390–5

Roberts, J. A., Roger, R. S., Ribes, J.-C., Cooke, D. J., Murray, J. D., Cooper, B. F. C., and Biraud, F. 1975 Measurements of circular polarisation of radio sources at frequencies of $0\cdot63$, $1\cdot4$, $5\cdot0$ and $8\cdot9$ GHz *Aust. J. Phys.* **28**, 325–51

Shapirovskaya, N. Ya. 1978 Variabiliy of extragalactic decimeter radio sources *Soviet Astron. AJ* **22**, 544–7

Sieber, W. 1982 Causal relationship between pulsar long-term intensity variations and the interstellar medium *Astron. Astrophys.* **113**, 311–13

Tatarski, V. I., and Zavorotnyi, V. U. 1980 Strong fluctuations in light propagation in a randomly inhomogeneous medium *Prog. Optics* **18**, 204–56

Taylor, J. H., and Cordes, J. M. 1993 Pulsar distances and the Galactic distribution of free electrons *Astrophys. J.* **411**, 674–84

Uscinski, B. J. 1977 The Elements of Wave Propagation in Random Media McGraw–Hill (New York)

Wagner, S. J., and Witzel, A. 1995 Intraday variability in quasars and BL Lac objects *Ann. Rev. Astron. Astrophys.* **33**, 163–97

Walker, M. A. 1998 Interstellar scintillation of compact extragalactic radio sources *Mon. Not. R. Astron. Soc.* **294**, 307–11

Walker, M., and Wardle, M. 1998 Extreme scattering events and Galactic dark matter *Astrophys. J.* **498**, L125–9

Wolszczan, A., and Cordes, J. M. 1987 Interstellar interferometry of the pulsar PSR 1237+25 *Astrophys. J.* **320**, L35–9

Appendix A: Scattering in a Birefringent Medium

The theory of strong scattering is generalised to an anisotropic medium in the case where the propagation of the two natural modes may be treated independently.

In a weakly anisotropic medium there are two wave modes with approximately transverse, orthogonal polarisations. Waves in these two modes propagate independently of each other provided that the medium is homogeneous, and this continues to be the case in a weakly inhomogeneous except near 'coupling points' where the two modes are degenerate and coupling between them needs to be taken into account. Such mode coupling is ignored here. The treatment of the transfer of radiation then involves separating the incident radiation into components in the two modes, treating the propagation of the two modes independently, and combining the components again at the image plane.

As in Section 2, let the mean ray direction be along the z axis. The transverse (x and y) components are denoted by greek superscripts, and the two modes are labelled $\sigma = \pm$, with wavenumber k_σ. The amplitude E^α is written as the sum of components $u_\sigma(z, \mathbf{r}) e^\alpha_\sigma \exp(ik_\sigma z)$ in the two modes, with e^α_σ the (unimodular) polarisation vector. The wave equation, generalising (2·2), is

$$\left(\nabla^2 \delta^{\alpha\beta} + \frac{\omega^2}{c^2} K^{\alpha\beta}\right)(u^\beta e^{ik_\sigma z}) = 0, \qquad (\mathrm{A}\cdot 1)$$

which is solved for the eigenvalues $k = k_\sigma$ and the eigenfunctions e^α_σ. Initially the turbulence is ignored. This involves writing $K^{\alpha\beta} = \langle K^{\alpha\beta}\rangle + \delta K^{\alpha\beta}$ and retaining only the average part of the the response tensor, $\langle K^{\alpha\beta}\rangle$. The polarisation vectors are orthogonal elliptical of the form

$$\mathbf{e}_\sigma = (1, iT_\sigma), \qquad T_+ T_- = -1, \qquad (\mathrm{A}\cdot 2)$$

where T_σ is the axial ratio of the polarisation ellipse (with the sign denoting the handedness of the circular polarisation).

The parabolic approximation to (A·1) is

$$\left(2ik_\sigma \frac{\partial}{\partial z} + \nabla^2_\perp + \frac{\omega^2}{c^2}\delta K_\sigma\right) u_\sigma = 0, \qquad (\mathrm{A}\cdot 3)$$

with $\delta K_\sigma = e^{*\alpha}_\sigma e^\beta_\sigma \delta K^{\alpha\beta}$. The solution of (A·3) in the absence of the term δK_σ is

$$u_\sigma(z, \mathbf{r}) = -\frac{ik_\sigma}{2\pi(z - z')} \int d^2\mathbf{r}'\, u_\sigma(z', \mathbf{r}') \exp\left[\frac{ik_\sigma(\mathbf{r} - \mathbf{r}')^2}{2(z - z')}\right], \qquad (\mathrm{A}\cdot 4)$$

which generalises (2·3). Similarly,

$$u_\sigma(L, \mathbf{r}) = -\frac{i}{2\pi r^2_{\mathrm{F}\sigma}} \int d^2\mathbf{r}' u_\sigma(0, \mathbf{r}') \exp\left[i\frac{(\mathbf{r} - \mathbf{r}')^2}{2r^2_{\mathrm{F}\sigma}}\right] \qquad (\mathrm{A}.5)$$

generalises (2·4) with (2·5) generalised to

$$r_\sigma = (L/k_\sigma)^{\frac{1}{2}}. \tag{A·6}$$

On including the term involving δK_σ in (A·3), a perturbation expansion gives (A·4) as the zeroth order solution, and the first order solution is

$$u_\sigma^{(1)}(z,\mathbf{r}) = \frac{\omega^2}{4\pi c^2}\int_0^z \frac{dz'}{z-z'}\int d^2\mathbf{r}'\,\delta K_\sigma(z',\mathbf{r}')u_\sigma(z',\mathbf{r}')\,\exp\left[\frac{ik_\sigma(\mathbf{r}-\mathbf{r}')^2}{2(z-z')}\right]. \tag{A·7}$$

The generalisation of (2·6) is

$$u_\sigma(z,\mathbf{r}) = -\frac{ik_\sigma e^{ik_\sigma(z-z')}}{2\pi(z-z')}\int d^2\mathbf{r}'\,u_\sigma(z',\mathbf{r}')\,e^{i\phi_\sigma(\mathbf{r})}\,\exp\left[\frac{ik_\sigma(\mathbf{r}-\mathbf{r}')^2}{2(z-z')}\right], \tag{A·8}$$

where the phase $\phi_\sigma(\mathbf{r})$ includes the effects of the fluctuations at the screen. The statistical average over the phases is performed assuming gaussian phases with, in place of (2·7),

$$\langle e^{i[\phi_\sigma(\mathbf{r})-\phi_{\sigma'}(\mathbf{r}')]}\rangle = e^{-D_{\sigma\sigma'}(\mathbf{r}-\mathbf{r}')/2}, \tag{A·9}$$

where $D_{\sigma\sigma'}$ is the phase structure function. The mutual coherence function generalises to

$$\langle I_{\sigma\sigma'}(z,\mathbf{r}-\mathbf{s})\rangle = \frac{k_\sigma k_{\sigma'}}{(2\pi)^2 z^2}\int d^2\mathbf{r}'d^2\mathbf{s}'\,\langle I_{\sigma\sigma'}(0,\mathbf{r}'-\mathbf{s}')\rangle\,e^{-D_{\sigma\sigma'}(\mathbf{r}'-\mathbf{s}')/2}$$
$$\times\exp\left[i(k_\sigma-k_{\sigma'})z + \frac{ik_\sigma(\mathbf{r}-\mathbf{r}')^2 - ik_{\sigma'}(\mathbf{s}-\mathbf{s}')^2}{2z}\right]. \tag{A·10}$$

For $\sigma \neq \sigma'$ the phase factor $(k_\sigma - k_{\sigma'})z$ describes the effects of Faraday rotation in the case of circularly polarised wave modes.

The fourth order moment in general involves four different positions (ρ_1, ρ_2, ρ_1', ρ_2' say). The only case considered here is for the correlation in the intensities in the two modes. For an incident plane wave the fourth order moment can depend only on two combinations of the locations of the four fields on the wave screen. Specifically, one has

$$\Gamma_{\sigma\sigma'}(z,\mathbf{r}_1,\mathbf{r}_2) = \langle u_\sigma(z,\rho_1)u_{\sigma'}(z,\rho_2)u_\sigma^*(z,\rho_1')u_{\sigma'}^*(z,\rho_2')\rangle, \tag{A·11}$$

$$\mathbf{r}_1 = \tfrac{1}{2}(\rho_1-\rho_2+\rho_1'-\rho_2'),$$
$$\mathbf{r}_2 = \tfrac{1}{2}(\rho_1-\rho_2-\rho_1'+\rho_2'). \tag{A·12}$$

In the case of a thin screen, the solution for this quantity is

$$\Gamma_{\sigma\sigma'}(z,\mathbf{r}_1,\mathbf{r}_2) = \left(\frac{k}{2\pi z}\right)^2 \int d^2\mathbf{r}_1' d^2\mathbf{r}_2' \,\langle I^2\rangle(0)$$

$$\times \exp\left[\frac{ik(\mathbf{r}_1-\mathbf{r}_1')\cdot(\mathbf{r}_2-\mathbf{r}_2')}{z} - G_{\sigma\sigma'}(\mathbf{r}_1,\mathbf{r}_2)\right],$$

$$\begin{aligned} G_{\sigma\sigma'}(\mathbf{r}_1,\mathbf{r}_2) = & -D_{\sigma\sigma'}(\mathbf{r}_1+\mathbf{r}_2) + 2D_{\sigma\sigma'}(\mathbf{r}_2) + 2D_{\sigma\sigma'}(\mathbf{r}_1) \\ & + D_{\sigma'\sigma'}(\mathbf{r}_2) - D_{\sigma\sigma'}(\mathbf{r}_1-\mathbf{r}_2) \\ & - 2D_{\sigma\sigma'}(\mathbf{r}_2) + D_{\sigma\sigma}(\mathbf{r}_2) + D_{\sigma'\sigma'}(\mathbf{r}_2). \end{aligned} \tag{A·13}$$

The fact that the phase structure function is an even function implies

$$\Gamma_{\sigma\sigma'}(z,\mathbf{r}_1,\mathbf{r}_2) = \Gamma_{\sigma'\sigma}(z,\mathbf{r}_2,\mathbf{r}_1). \tag{A·14}$$

The intensity fluctuations may be described in terms of the power spectrum, $W_{\sigma\sigma'}(\mathbf{q})$, by writing

$$\Gamma_{\sigma\sigma'}(z,\mathbf{r}_1,\mathbf{0}) = \int d^2\mathbf{r}_1\, e^{i\mathbf{q}\cdot\mathbf{r}_1}\, W_{\sigma\sigma'}(\mathbf{q}), \tag{A·14}$$

which generalises (2·13).

Appendix B: Scattering by Discrete Objects

Consider N scatterers with the ith scatterer at $\mathbf{r}=\mathbf{r}_i$ and described by some set of parameters, α_i, that includes its size, shape, orientation, density profile and so on. Then $\Delta\phi_i f_i(\mathbf{r}-\mathbf{r}_i)$ in equation (6·1) may be replaced by $\Delta\phi_0 f(\mathbf{r}-\mathbf{r}_i;\alpha_i)$, so that equation (6·1) becomes

$$\Delta\tilde{\phi}(\mathbf{q}) = \sum_{i=1}^{N} \Delta\phi_0\, \tilde{f}(\mathbf{q};\alpha_i)\, e^{-i\mathbf{q}\cdot\mathbf{r}_i}. \tag{B·1}$$

Correspondingly, (6·4) is replaced by

$$\tilde{C}(\mathbf{q}) = \sum_{i,j=1}^{N} \frac{(\Delta\phi_0)^2}{A}\, \tilde{f}_i(\mathbf{q},\alpha_i)\tilde{f}_j^*(\mathbf{q},\alpha_j)\, e^{-i\mathbf{q}\cdot(\mathbf{r}_i-\mathbf{r}_j)}. \tag{B·2}$$

The next step is to average equation (B·2) over the distribution of discrete objects.

Suppressing the parameters α_i for the present, to describe the distribution of locations of the objects in equation (B·2), let $p(\mathbf{r}_1,\ldots,\mathbf{r}_N)\, d^2\mathbf{r}_1\ldots d^2\mathbf{r}_N$ be the probability that the N scatterers are in the regions $d^2\mathbf{r}_1,\ldots,d^2\mathbf{r}_N$. The probability for a single scatterer, $p(\mathbf{r}_1)$, is obtained from $p(\mathbf{r}_1,\ldots,\mathbf{r}_N)$ by integrating over $d^2\mathbf{r}_2\ldots d^2\mathbf{r}_N$. The probability function for a pair of scatterers, $p(\mathbf{r}_1,\mathbf{r}_2)$, is obtained from $p(\mathbf{r}_1,\ldots,\mathbf{r}_N)$ by

integrating over $d^2\mathbf{r}_3 \ldots d^2\mathbf{r}_N$. For a distribution that is random, there is only one nontrivial probability function, $p(\mathbf{r})$, and all the other probability functions are outer products of it. Specifically, one has $p(\mathbf{r}_1, \ldots, \mathbf{r}_N) = p(\mathbf{r}_1) \ldots p(\mathbf{r}_N)$. For a uniform distribution over an area A, one has $p(\mathbf{r}) = 1/A$. The two-point correlation function, defined by

$$g(\mathbf{r}_1 - \mathbf{r}_2) = p(\mathbf{r}_1, \mathbf{r}_2) - p(\mathbf{r}_1)p(\mathbf{r}_2), \tag{B·3}$$

is a measure of nonuniformity in the spatial distribution of objects.

The parameters α_i describe the size, shape, and so on, and the averages over these parameters are assumed statistically independent of each other and of the average over locations. Let $d\alpha_i$ denote the product of infinitesimal ranges of each of these parameters. The probability distribution for the locations introduced above then becomes the generalised probability distribution $p^N = p(\mathbf{r}_1, \ldots, \mathbf{r}_N; \alpha_1, \ldots, \alpha_N)$, which is the probability that the N scatterers are in the regions $d^2\mathbf{r}_1, \ldots, d^2\mathbf{r}_N$ and the parameter ranges $d\alpha_1, \ldots, d\alpha_N$. The probability for a single scatterer, $p(\mathbf{r}_1; \alpha_1)$, is obtained by integrating p^N over $d^2\mathbf{r}_2 \ldots d^2\mathbf{r}_N d\alpha_2 \ldots d\alpha_N$. The probability function for a pair of scatterers, $p(\mathbf{r}_1, \mathbf{r}_2; \alpha_1, \alpha_2)$, is obtained by integrating p^N over $d^2\mathbf{r}_3 \ldots d^2\mathbf{r}_N d\alpha_3 \ldots d\alpha_N$.

The averages over the parameters α_i may be performed over equation (B·1) directly. Denoting the average by a tilde, we have

$$\Delta\tilde{\phi}(\mathbf{q}) = \sum_{i=1}^{N} \Delta\phi_0 \int d\alpha_i \, \tilde{f}(\mathbf{q}; \alpha_i) \, e^{-i\mathbf{q}\cdot\mathbf{r}_i}. \tag{B·4}$$

These averages may then be combined with the average over locations trivially.

Manuscript received 29 September, accepted 14 December 1998